Excited-state photoelectron spectroscopy of excitons in C_{60} and photopolymerized C_{60} films

J. P. Long, S. J. Chase,* and M. N. Kabler
Naval Research Laboratory, Washington, DC 20375
(Received 17 May 2001; published 2 November 2001)

Laser-excited states in films of pristine C_{60} and photopolymerized C_{60} (pp-C_{60}) prepared in ultrahigh vacuum have been characterized *in situ* with pump-probe photoelectron spectroscopy using both synchrotron radiation and picosecond laser sources. Photoelectron spectra of singlet (S_1) and triplet (T_1) excitons overlap because of vibrational broadening in the photoemission final state. The spectra have been individually isolated in pp-C_{60} with time-resolved methods and are split by 0.33 eV. Signals from pristine C_{60} are weaker but are spectroscopically similar. The origin for exciton transitions for both C_{60} and pp-C_{60} is found to be properly located near the maximum of the highest occupied molecular orbital. Increasing excitation density favors T_1 production over S_1 such that, at high exciton concentrations, T_1 states predominate, even at times much shorter than the unimolecular intersystem crossing time, measured to be ~2.5 ns for pp-C_{60} at 81 K. A weaker photoemission band located ~0.5 eV above S_1 is also observed and is attributed to charge carriers and/or charge-transfer excitons.

DOI: 10.1103/PhysRevB.64.205415 PACS number(s): 71.20.Tx, 71.35.Gg, 72.80.Rj, 79.60.−i

I. INTRODUCTION

In molecularly based electronic devices, the simultaneous presence of localized excitations, such as singlet and triplet excitons and polarons, complicates photophysical behavior[1] and might degrade performance through mutual annihilation.[2] Considerable effort has therefore been directed towards understanding the nonequilibrium species in molecular materials.[3] Numerous techniques have been employed, including transient optical absorption, luminescence, photoconductivity, and optically detected magnetic resonance. However, comprehensive studies of the interactions among excited states are in general limited by the difficulty of simultaneously detecting the various excited species with comparable sensitivity and time resolution. Hence even for a material as well studied as C_{60}, questions remain concerning the nature of the photoexcited states and their dynamical interactions.[4]

Excited-state photoelectron spectroscopy (ESPES) offers distinct advantages in that it can provide a direct means of probing all nonequilibrium species containing an electron. With ESPES, one first photoexcites a nonequilibrium electron population and then photoemits a portion of it into vacuum, where its energy distribution and amplitude are sampled with an electron spectrometer. By using pulsed sources and following the amplitude as the delay between pump and probe is varied, dynamical information can be obtained. Molecular materials are especially amenable to this technique because the magnitudes of exciton binding energies and singlet-triplet splittings are, in many cases, large enough to observe with ordinarily available spectral resolution.

Early applications of ESPES to molecular films included cw experiments on polyacetylene[5] and pulsed experiments on several materials.[6] Subsequently, ESPES has been applied primarily to covalent semiconductors and metals as recently reviewed.[7,8] However, its application to excited states in molecular films is presently attracting increasing attention,[9–16] particularly for the case of fullerenes.[9–11,14,16]

Here we describe in some detail the photoelectron spectroscopy of excitons in films of C_{60} and photopolymerized C_{60} prepared in ultrahigh vacuum and studied *in situ*. Hereafter we will designate the pristine (as deposited) films as C_{60} and the photopolymerized films as pp-C_{60}. Treatment of the dynamical behavior is postponed for a later publication but both the spectroscopy and dynamics were described briefly in a prior submission.[17] We treat pp-C_{60} more extensively because it yielded larger excited-state signals. We used to advantage two different setups, one based on a copper-vapor laser pump and synchrotron radiation (SR) probe,[18] the other employing laser-radiation (LR) harmonics (Nd:YAG laser) as both pump and probe.

The SR setup not only provided pulsed operation with subnanosecond resolution, but also allowed effective cw operation with gated detection at microsecond delays between laser pump and SR probe. This permitted a spectrum of the lowest-energy triplet exciton T_1 to be isolated and unambiguously identified on the basis of its long lifetime. The SR setup also provided placement of the exciton spectrum relative to the highest occupied molecular orbital (HOMO), as shown in Fig. 1. With the ~90-ps resolution provided by the LR setup, a spectrum of the lowest-lying singlet exciton S_1 was isolated by probing at times less than the unimolecular intersystem crossing time ~2.5 ns in pp-C_{60} at 81 K. We thus were able to identify both S_1 and T_1 features with high confidence (Fig. 1). The LR experiment also revealed a transient population of higher states near the bottom of the lowest unoccupied molecular orbital (LUMO), ~0.5 eV above S_1. These states probably originate from free or trapped carriers or, possibly, charge transfer excitons.

The spectral features we have observed generally correspond to those of recent femtosecond investigations of pp-C_{60} films.[11,16] However, our assignments to particular excited states differ by being offset by one component. For example, our long-lived T_1 feature was attributed to S_1 in the previous work. Also, we have located the origin S_0 for exciton transitions at an energy near the top of the HOMO rather than the center.

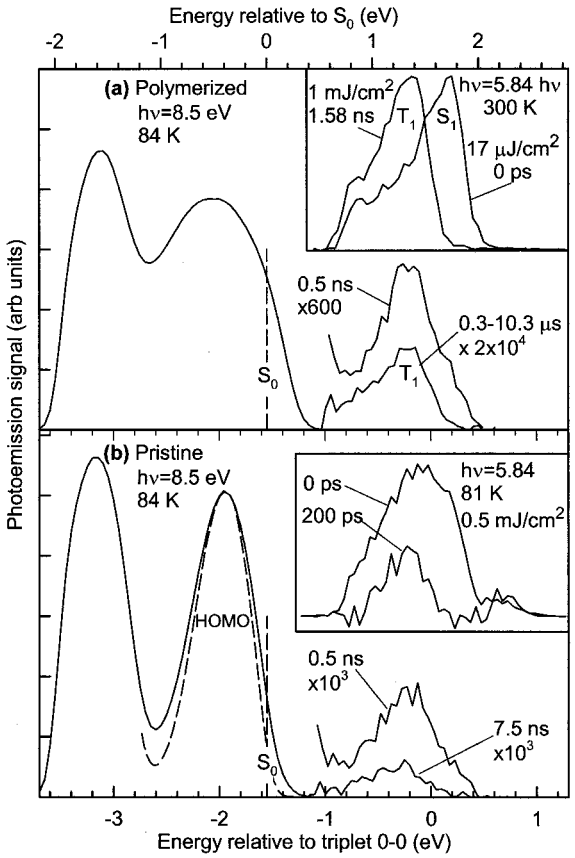

FIG. 1. Photoelectron spectra of valence states and background-subtracted excited states, probed at the specified delays with two sources: nanosecond synchrotron (main panels, 2.8 mJ/cm^2) and picosecond laser (insets). In the bottom axis, zero energy is the estimated 0-0 line of the T_1 exciton; in the top axis, zero is the inferred origin of transitions (S_0) discussed in the text. (a) Photopolymerized C_{60} (pp-C_{60}). Note pure T_1 spectrum accumulated 0.3 to 10.3 μs after the 5-ns pump pulse. The 0.5-ns spectrum comprises both S_1 and T_1. (b) Pristine C_{60}. The dashed HOMO was acquired with higher energy resolution than all other spectra. Insets: (a) pp-C_{60} comparing normalized S_1 at low fluence and nearly pure T_1 remaining after high-fluence dynamic interactions. (b) Unnormalized pristine C_{60} exciton spectra at two time delays.

We also discuss the dependence of the exciton spectra on pump-laser fluence and on the delay time of the probe after the pump. An interesting result is that as fluence increases and excited-state concentrations exceed $\sim 10^{19}\,\mathrm{cm}^{-3}$, the T_1 concentration is enhanced for times much less than the intersystem crossing time while the S_1 population tends to saturate. Previously, to explain room-temperature measurements of transient absorption in C_{60} films exposed to air, an increased rate of T_1 production at high fluence was proposed, but the roles of S_1 and T_1 could not be separated.[19] Recently, a similar preferential growth in T_1 states at high excitation density was reported for the conjugated oligomer *para*-hexaphenyl.[2]

Accompanying the enhanced T_1 production at high excitation densities in C_{60} and pp-C_{60}, we find complex transient behavior, which includes an increase in the decay rates of both T_1 and S_1 with excited state concentration, always with S_1 decaying more rapidly. Complex transient decays in pp-C_{60} have been noted previously on the basis of four-wave mixing experiments sensitive to a composite of excited-state species.[20] By spectroscopically distinguishing the populations of S_1 and T_1 excitons, we are able to characterize their dynamics independently.

These measurements have provided extensive data concerning the temporal and pump-fluence dependencies of S_1 and T_1 exciton concentrations. This has facilitated development of a dynamical model, expressed through coupled rate equations, that incorporates annihilation interactions among the three primary excited species, namely, S_1 and T_1 excitons and free carriers, and thus goes beyond previous, simpler models. This model has been described briefly[17] and will be reported in detail in a subsequent manuscript.

II. EXPERIMENT

The combined SR-laser system[18,21] was located at beamline X24C at the National Synchrotron Light Source, Brookhaven National Laboratory. There the pump-laser source was a copper-vapor laser ($h\nu = 2.43$ eV) operating at 6 kHz and configured with competing cavities to produce 5-ns pulses full width at half maximum (FWHM). The laser was triggered with a signal derived from electrodes sensing the electron bunches circulating in the storage ring. Spatial and time overlap of the SR pulses and laser pulses were aided with use of visible SR obtained by operating the monochromator grating in zero order. Spatial overlap was achieved visually by steering the weakly focused, ~3-mm diameter laser spot to overlap the zero-order SR spot. To check spot overlap at *operating* wavelengths, a 1-mm diameter pinhole was centered on the 1-mm×1.2-mm SR spot by minimizing the pinhole's photoemission, and then the laser spot was adjusted to the pinhole. Laser fluence was calibrated by measuring the power transmitted through the calibrated area of the pinhole. Time overlap was aided by using an avalanche photodiode to simultaneously sample both the 5-ns laser pulse and the subnanosecond, zero-order SR pulse, after both beams had passed through the pinhole. Coincidence was then obtained by observing an oscilloscope while adjusting the timing of the laser trigger with an electronic delay generator in combination with passive delays. These delays were subsequently varied to map out excited-state decays.

A SR photon energy $h\nu$ of 8.5 eV was selected to produce the largest excited state signals within the range tested, 7.5–10.5 eV. The selected $h\nu$ reflects primarily the beamline transmission, including that of a LiF filter inserted into the beam to eliminate higher-order grating harmonics. Without the LiF filter, emission from these harmonics would overwhelm the weak ESPES signals, which typically produced count rates less than 1 Hz (see Fig. 2). Attempts were made to employ larger $h\nu$'s in order to record spectra with more surface-sensitive photoelectron energies for comparison and in order to exploit possible photoemission resonances.[22,23] Above the LiF cutoff, second-order grating harmonics were suppressed by edge absorption in Sn or In thin-film transmission filters and by reflection from a critical-angle (low-pass)

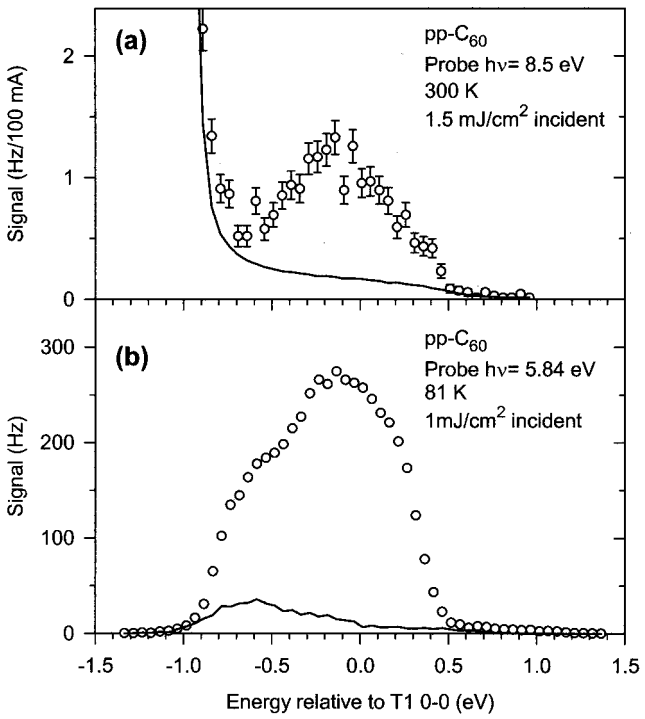

FIG. 2. Solid lines: background emission measured with pump-laser off. Symbols: total emission with pump and probe coincident in time. (a) Synchrotron radiation probe; count rate is normalized to 100 mA of current in the storage ring, the maximum available in the special single-bunch operating mode best suited for maximizing signal at high time resolution (Ref. 18). Error bars give ±one standard deviation from counting statistics. (b) Probe is the Nd:YAG laser fifth harmonic.

mirror of oxide-free silicon.[24] For detailed spectroscopy, however, the metal filters reduced signals to impractical levels and the mirror was unable to suppress the second-order grating harmonic sufficiently.

The storage ring was operated in two modes. In single-bunch mode, with which most of the data were taken, only one electron bunch circulated in the storage ring, producing ~0.6-ns SR pulses at a 1.76-MHz repetition rate. This mode maximized the number of SR photons per pulse ($\sim 5 \times 10^4$/pulse) and hence maximized the number of photons coincident with the exciting laser pulse. For pump-probe experiments, single-bunch operations also enabled the best time resolution, which was limited by laser jitter to ±0.5 ns. In the second mode of operation, 25-bunch mode, the laser was desynchronized so that, in effect, SR served as a cw source. In this mode, time resolution was limited to ~12 ns by transit-time dispersion of the various electron trajectories within the electron spectrometer.[18] For times greater than ~50 ns after the pump pulse, this mode could provide an improved data rate because larger currents were stored in the ring and because longer gate times could be used without distorting the slower decays in this time regime.

The picosecond laser setup at the Naval Research Laboratory (NRL) used the Nd:YAG laser second harmonic ($h\nu = 2.33$ eV) as pump and the fifth harmonic ($h\nu = 5.84$ eV) as probe. The laser was mode-locked and simultaneously *Q*-switched at a 2-kHz repetition rate. A Pockels cell plucked for use the most intense mode-locked pulse from each *Q*-switched envelope. The harmonics were generated by three crystals placed sequentially after the Pockels cell: CD**A* to produce the second, KTP the fourth, and BBO the fifth in a 4+1 mixing scheme.[25] A fused silica prism separated the harmonics. From autocorrelation measurements of the plucked fundamental pulse, we infer FWHM durations of 75 ps for the pump and 50 ps for the probe. Pump and probe beams were independently attenuated and focused, respectively, to 380 and 80 μm FWHM. Pump-laser fluences were calibrated by measuring the power transmitted through a pinhole of measured area. Spatial overlap was optimized by steering the pump beam for maximum excited-state signal. The relative timing of the probe was controlled with an optical delay line.

For both the SR and LR setups, C_{60} films were sublimed in ultrahigh vacuum onto room-temperature substrates from powder[26] outgassed at 100 to 200 °C for several hours prior to each evaporation. The substrates were made of oxygen-free high-conductivity copper polished to a mirror finish and cleaned *in situ* by Ar-ion bombardment until a sharp Fermi edge resulted. The deposition rate was typically 2 nm/min. Film thickness was varied from 42 to 84 nm as measured with a quartz crystal oscillator. Films were polymerized *in situ* by exposure at room temperature to the pump-laser radiation at doses from 15 to 20 kJ/cm^2, delivered with fluences from 1.6 to 3 mJ/cm^2 per pulse. At NSLS, polymerization was monitored by characteristic changes in the valence band.[27] At both NSLS and NRL similar doses were employed and polymerization was verified by the insolubility of exposed spots in toluene. Because polymerization proceeded too rapidly at room temperature to allow data to be obtained from unmodified material, pristine films had to be studied at 81–84 K, where polymerization rates proved undetectable.[27] Polymerized films were investigated at both room temperature and 81–84 K.

In both setups, photoelectron energy distributions were measured with a double-pass cylindrical mirror analyzer (CMA) operating with constant energy resolution. Resolution was determined by fitting the Fermi edge that was routinely recorded from the copper substrates. Resolution in the LR experiments ranged between 0.16 and 0.20 eV; in the SR experiments, the pass band was increased to 0.18 to 0.22 eV because of the weaker signals. Samples were biased from −5 to −10 V to ensure collection of the low-energy electrons; spectral shapes were unchanged over this bias range. Samples were oriented with the surface normal directed into the acceptance annulus of the CMA. Angles of incidence relative to the normal for the probe (pump) beams were 33° (35°) in the SR setup and 48°(55°) in the LR setup. All beams were *p* polarized. Data acquisition with SR employed a time-to-digital converter to histogram the time that each photoelectron arrived within a specified period around each laser pulse.[18] Concurrently, photoelectrons were also counted in a 100-μs window ending just prior to the laser pulse in order to acquire ''laser-off'' spectra. With the LR setup, photoelectrons were simply counted within a 500-ns window that bracketed the probe pulse to reduce dark counts.

In the LR experiments, probe fluence was maintained below 0.7 μJ/cm^2 to prevent self-pumping, detectable as a weak superlinear dependence on probe fluence of a background signal discussed below. For the SR experiments, linear conditions prevailed because the incident probe fluence was orders of magnitude weaker ($\leqslant 4\times 10^6$ photons/cm^2 per pulse in single-bunch operations as calibrated from the photocurrent emitted from a sputtered gold foil[28]).

Pump beams, and the probe beam in the LR setup, were variably attenuated by using a half-wave plate to rotate the plane of polarization relative to the plane of transmission of a polarizing prism. Comparable pump fluences were employed in both setups: 0.04 to 2.8 mJ/cm^2 in the SR setup and 0.017 to 1.6 mJ/cm^2 in the LR setup. Temperature transients in the films were calculated with a finite-element code[29] that incorporated the temperature-dependent thermal properties of C_{60} (Refs. 30, 31) and the spatial profile of volumetric absorption determined with thin-film optical calculations.[32] At the highest fluences, the maximum transient temperatures for the SR data were calculated to be 345 and 117 K for initial temperatures of 295 and 84 K, respectively. For the LR data, the maximum temperatures were 335 and 185 K for initial values of 295 and 81 K.

Use of SR permitted checking the valence band for the presence of transient photovoltages.[33] The pump pulse produced small photovoltages that varied among films from -40 to $+10$ meV, but in the great majority of cases was about -20 meV. In Figs. 1 and 2(a), ground state emission from the valence band is shown at the energy it appeared *during* the pump pulse.

III. RESULTS AND DISCUSSION

A. Spectral features and assignments

Figure 1 summarizes ESPES spectra for C_{60} and photopolymerized (pp-C_{60}) films recorded with synchrotron radiation (SR; main panels) and laser radiation (LR; insets). Because of its higher probe $h\nu$, SR produces emission from both valence and excited states, so that a common energy axis obtains. The bottom axis of the plot has its zero of energy at the 0-0 photoemission transition of the T_1 state, located as described below. Included at the top is a second scale with its zero at the S_0 origin, obtained by subtracting from the $T_1$0-0 position an energy of 1.54 eV (discussed below) for the $S_0 \rightarrow T_1$ transition. Laser-excited states appear at energies above the HOMO. The strongest excited-state emission occurs below the Fermi level E_F, which fell between 0.3 and 0.4 eV for all SR and LR experiments. For *nonequilibrium* states falling well below E_F, excitonic character is implicated.

The polymerization-induced changes in the C_{60} valence band shown in Fig. 1 have been discussed previously.[27] The changes are consistent with calculations[34] of the electronic structure for a C_{60} dimer formed through a four-member ring, the bonding arrangement of the $2+2$ cycloaddition reaction believed to be responsible for photopolymerization.[35] In a three-dimensional film, multiple coordination becomes possible. For instance, analysis of C-1s photoemission lineshapes in films identically polymerized suggest a mean coordination of three in our samples.[27] Given the statistical process by which rotating C_{60} molecules come into proper alignment for $2+2$ cycloaddition,[35] uniform coordination is unlikely and pp-C_{60} should exhibit covalent intermolecular-bonding disorder that is absent in C_{60}. Some additional inhomogeneous broadening in pp-C_{60} is consequently likely. In spite of the significant differences between the valence spectra of C_{60} and pp-C_{60}, the excited-state spectra are markedly similar, as described below.

In Fig. 1, a weak background has been subtracted from each excited-state spectrum. The background was present for both LR and SR probes acting alone, as illustrated in Fig. 2, and has been subtracted in all other spectra reported here. Although the background has not been studied in detail, we remark on it as follows. At low temperatures, it slowly increased with ultraviolet (UV) exposure and so was recorded periodically. That part of the background emission that grew with UV dose could be substantially annealed away by warming the film to room temperature and may represent metastable surface or bulk traps created by UV exposure and stabilized by low temperature. The emission often extended above E_F a few tenths of an eV and fell off more gradually than expected for a Fermi cutoff. Emission above E_F might reflect slow equilibration times for some trapped electrons. At low temperature, the background grew with UV exposure more rapidly in C_{60} than pp-C_{60}, suggesting that some traps might arise from light-induced disordering of the orientational order that freezes in at $\sim$90 K.[36] Also, in contrast to pp-C_{60}, the background in C_{60} was transiently perturbed during laser pumping with the LR setup. This effect is responsible for negative features in the baseline of the background-subtracted, 200-ps spectrum in the inset of Fig. 1(b).

Care must be exercised when regarding the lowest kinetic energies of the excited-state spectra. The SR measurements show that the HOMO emission slopes steeply with energy where it merges with the lowest laser-induced emission [Fig. 2(a)] and this slope decreases slightly during laser pumping. Below about -0.7 eV in Fig. 1, this line shape change introduces additional sensitivity to small errors in accounting for the weak photovoltage shift when subtracting laser-off from laser-on spectra. In the case of LR, details at the lowest energies were affected by the vacuum cutoff. In spite of these complications, line-fitting analysis indicates the presence of a third pumped component (in addition to S_1 and T_1) below T_1 which blends into the HOMO. This component may represent ground state molecules perturbed by nearby excited states as discussed below.

The T_1 exciton spectrum was identified by using SR to accumulate the excited state signal during the period 0.3 to 10.3 μs after the 5-ns laser pulse. These times far exceed the $\sim$1.3-ns unimolecular lifetime measured for S_1, so that only triplets could possibly be present in quantity at energies below E_F. The unimolecular lifetime of T_1 was measured to be $\sim$15 μs for our pp-C_{60} films at 81 K. As the inset to Fig. 1(a) shows, an almost pure T_1 spectrum was also obtainable after only $\sim$1.5-ns delay with the LR setup if large enough pump fluences were used. This circumstance was brought about by the enhanced production of T_1 over S_1 at high

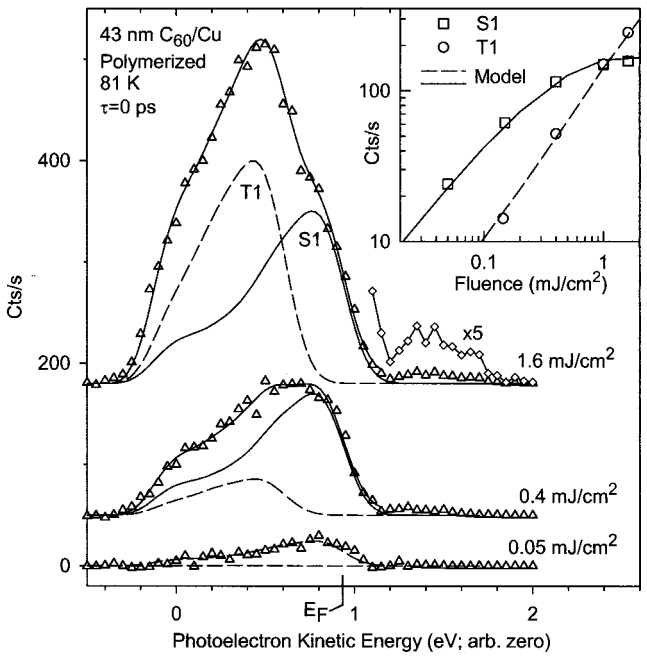

FIG. 3. Symbols: background-subtracted excited-state spectra for various incident fluences of the 75-ps pump laser when coincident with the probe pulse ($\tau=0$). Spectra are offset vertically for clarity. T_1 predominance at high fluence is evident as the increasing peak at 0.5 eV. E_F gives the measured Fermi level. The emission band above E_F is located approximately at the LUMO. Curves: fits of S_1 and T_1 contributions using an identical model line shape for both excitons as described in the text. Inset: Symbols give fluence dependence of S_1 and T_1 from the fitted components. Curves give results of a rate-equation model (Ref. 17).

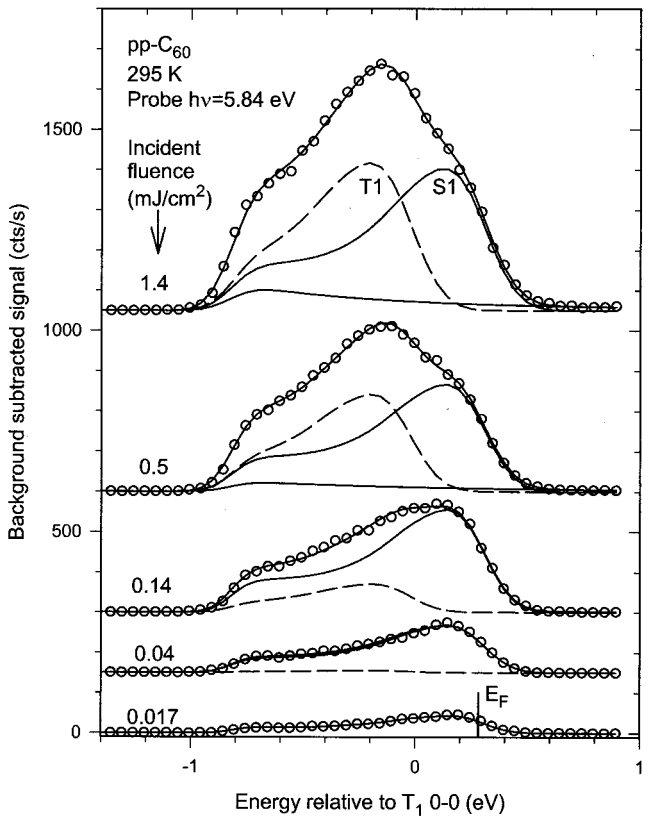

FIG. 4. Background-subtracted exciton spectra of a polymerized film at room temperature for various incident pump-laser fluences (symbols). Pump and probe were coincident in time. Spectra are offset vertically for clarity. Note similarity to behavior at 81 K, Fig. 3. Curves give fitted decomposition into T_1 and S_1 contributions and an exponentially falling component (not shown for lowest three spectra) that may reflect ground state molecules perturbed by adjacent excited molecules. The 0.017 mJ/cm^2 spectrum is pure S_1.

concentrations, together with a much more rapid S_1 decay at high concentrations. The close similarity of the T_1 spectra in Fig. 1, whether photoemitted with 5.84-eV LR or 8.5-eV SR, indicates that any differences in the photoelectron final state do not materially affect our results.

It also proved possible to observe an isolated S_1 spectrum if two criteria were satisfied. First was the need to probe before intersystem crossing could populate the spectrally overlapping T_1 population. Second, it proved crucial to use small enough pump fluences in order to avoid the concentration-induced production of T_1 *during* the 75-ps pump pulse. For example, in Figs. 3 and 4, which were recorded at zero time delay, the spectra for incident fluences below 0.05 mJ/cm^2 are essentially pure S_1. However, from the decomposition of the spectra into S_1 and T_1 components (obtained as described below), it is evident in Fig. 4 that by 0.14 mJ/cm^2 some T_1 contribution occurs in the middle of the spectrum. At 1.6 mJ/cm^2 the T_1 component is clearly predominant (Fig. 3).

Isolated T_1 and S_1 spectra recorded at 300 K with LR are normalized and compared in the inset to Fig. 1(a) and again in Fig. 5. Measurements at 81 K yielded identical shapes. By shifting the spectra for closest coincidence, we find T_1 lies 0.33 eV below S_1 for pp-C_{60}. This value is consistent with a splitting of 0.34 eV determined for pristine films with optical methods[37] and is slightly more than the 0.28–0.30 eV inferred by comparing electron energy loss and optical spectroscopies.[38–40]

A fourth, weak, transient photoemission band centered ~0.5 eV above S_1 was also observed (see Fig. 3, e.g.). This energy is near the lower edge of the LUMO, which is expected near 2.3 eV (Ref. 41) on the *top* axis in Fig. 1. It is likely these states originate from mobile or trapped electrons or from weakly bound charge-transfer excitons.[37,38] The weakness of this component in our data precluded a detailed characterization. Its magnitude suggests that the concentration of free or weakly bound electrons is significantly less than that of excitons. This is consistent with the small efficiency of photocarrier production in fullerene films, which has been explained[42,43] within the context of the Onsager model.[3,44,45] However, a quantitative comparison must acknowledge that the photoemission cross section for mobile carriers or charge-transfer excitons relative to Frenkel excitons is unknown and may depend strongly on the degree of localization. For example, within a model based on hydrogenic wave functions, the optical-absorption cross section for polarons falls markedly as the electron wave function becomes delocalized;[46] consequently the efficiency for photoemission from mobile or weakly bound carriers may be smaller than from more localized excitons.

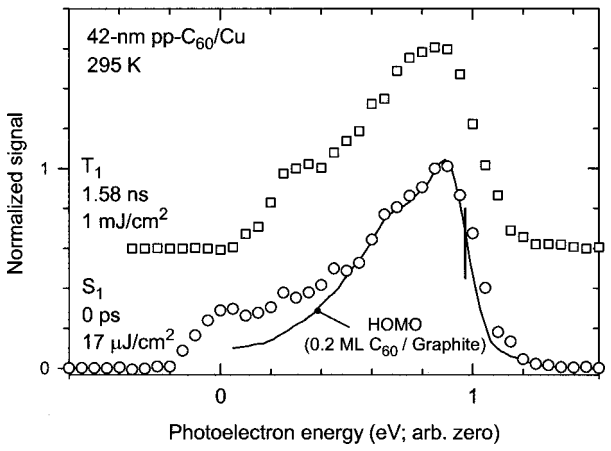

FIG. 5. Comparison of the S_1 and T_1 photoemission line shape to that of the HOMO from a 0.2 monolayer deposition of C_{60} on graphite (Ref. 53). No scaling of the energy axes has occurred but spectra have been aligned by eye and the T_1 spectrum is offset vertically for clarity. Vertical fiducial at 0.95 eV marks the approximate 0-0 line determined for the gas-phase HOMO (Ref. 53).

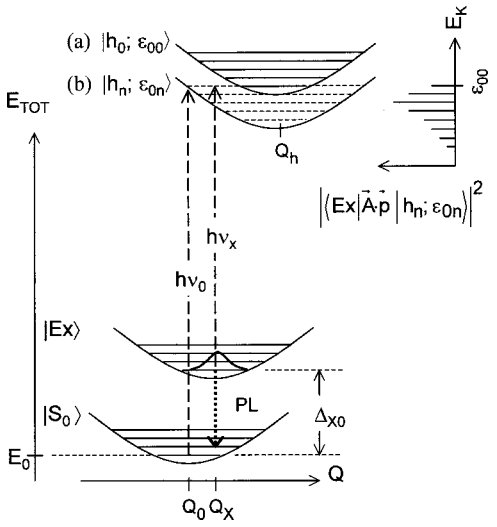

FIG. 6. Relevant transitions schematically represented by a conventional Frank-Condon diagram. Q is a generalized molecular configuration coordinate and $h\nu_x$ and $h\nu_0$ are probe photon energies. Exciton state *Ex* is shown in its vibrational ground state, as indicated by the Gaussian nuclear wave function. Two of many possible final photoemission states are shown as (a) and (b). In final state (a), the photohole h_0 is left on a molecule in its vibrational ground state and the outgoing photoelectron has energy ε_{00}. In (b), the molecule is left in vibrational state n ($n=4$ in the diagram) of energy $\hbar\omega_n$ and as a result the outgoing photoelectron has reduced kinetic energy $\varepsilon_{0n}=\varepsilon_{00}-\hbar\omega_n$. In this way, a monochromatic probe produces a vibrationally broadened photoelectron energy distribution as shown at the upper right.

The individual S_1 and T_1 line shapes measured for pp-C_{60} are much broader than the ~50 meV width predicted for free excitons,[38] even after considering our ~200 meV instrumental broadening. Inhomogeneous broadening should not be significant since vibrationally broadened S_1 photoluminescence from disordered C_{60} films[47,48] and pp-C_{60} (Refs. 49–51) exhibit an excess broadening relative to crystals[47,48,52] that is minor on our energy scale. In addition, unlike ESPES spectra from semiconductors, which show increasing signal to lower energies as electrons equilibrate at conduction or surface-state band edges,[7] these from pp-C_{60} exhibit a distinct decrease to lower energy, indicative of a vibrationally broadened line shape.

As shown in Fig. 5, each S_1 and T_1 photoemission spectrum closely resembles the vibrationally broadened HOMO spectrum of *isolated* C_{60} molecules in a 0.2-monolayer deposition on graphite (that, in turn, closely resembles the spectrum of gas-phase C_{60}).[53] The similarity demonstrates that the localized description of photoemission from C_{60} molecules also pertains to low lying excitons: the photohole is localized primarily on one molecule and broadening of the exciton's photoemission final-state results primarily from coupling of the hole to intramolecular vibrations. The situation is illustrated by the conventional Frank-Condon diagram[54,55] of Fig. 6, which schematically plots the total state-energies as a function of a generalized molecular configuration coordinate Q. Photoemission from an exciton state $|\mathrm{Ex}\rangle$ leaves the system in one of a number of possible vibrational final states, two of which are shown. In state (a) is depicted the final state produced by a 0-0 transition. Here the hole is left on a molecule in its vibrational ground state h_0 and the outgoing photoelectron has kinetic energy ε_{00}. In (b), the hole is left on a vibrationally excited molecule and the outgoing photoelectron, to conserve energy, has $\varepsilon_{0n}=\varepsilon_{00}-\hbar\omega_n$, where $\hbar\omega_n$ is the vibrational energy. Nonzero transition moments occur between $|\mathrm{Ex}\rangle$ in its vibrational ground state h_0 and the vibrationally excited final states because lattice relaxation around the photohole offsets the final state in Q to Q_h as drawn, giving finite vibrational matrix elements $\langle h_0|h_n\rangle$. In this way, a monochromatic probe $h\nu_x$ produces a vibrationally broadened exciton photoelectron energy distribution, as illustrated in the upper right corner of Fig. 6.

In Fig. 6, the total energy curve for the ground state S_0 is also shown offset in Q from the exciton, as is known to be the case for solid C_{60} because of vibronic structure in the S_1 photoluminescence[47–49,51,52] and in the electron-energy-loss spectroscopy (EELS) of T_1.[39,56–58] The vibrational structure observed in photoemission from isolated molecules[53] ($h\nu_0$ in Fig. 6) and its similarity to the exciton spectra (Fig. 5), compels the interpretation implicit in Fig. 6: both photoemissions create a similar, final hole state that is localized around one molecule. If the exciton curve is displaced in Q by a small amount relative to the photoemission final states, as shown, then the vibrational broadening can be approximately the same for S_0 and excitons as experiment requires, Fig. 5. Furthermore, this arrangement, with $(Q_h-Q_x)\approx(Q_h-Q_0)>(Q_X-Q_0)$, leads to a vibrationally broadened photoluminescence (for which the 0-0 transition is forbidden) that is much narrower than the vibrationally broadened photoemission, as observed for both disordered C_{60} films[47,48] and pp-C_{60} films.[49] The arrangement in Q is also consistent with the expectation that a relatively localized hole is more strongly coupled to nearby atoms than is a neutral exciton.

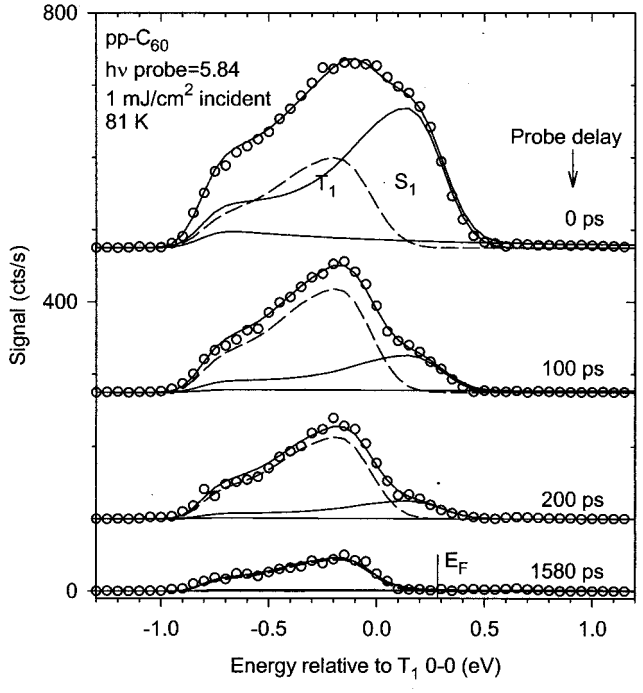

FIG. 7. Background-subtracted exciton spectra of a polymerized film at 81 K for various probe delays after the pump. Spectra are offset vertically for clarity. Decomposition into components is by fitting as in Fig. 3. Collision interactions produce a significant T_1 population even at 0 probe delay and lead to the loss of S_1 population much faster than its unimolecular lifetime at low concentrations of ~1.3 ns.

Among the final states available for photoemission from the HOMO in the solid state are those that dominate photoemission from the exciton, i.e., a localized hole and an outgoing photoelectron. Hence the exciton data support the view that vibrational broadening contributes significantly to the width of HOMO photoemission[53,57,59] in addition to any dispersive broadening from band structure.[58,60,61]

The evolution of the exciton spectra with pump fluence and probe delay can be reproduced as a linear combination of identically shaped S_1 and T_1 components, as illustrated in Figs. 3, 4, and 7. The component line shape was obtained by fitting the isolated S_1 spectrum with a model function $f(E)$. As a convenient means of introducing a suitable asymmetry, we based $f(E)$ on the low temperature theory[55] of optical transitions that are vibrationally broadened as described above in the context of the Frank-Condon picture, Fig. 6: $f(E)=\Sigma_n g\{[E-(\varepsilon_{00}-n\delta)]/W\}S^n/n!$, where g is the Gaussian function of width W, δ is the energy of the vibrational mode, ε_{00} is the 0-0 energy, S is the Huang-Rhys factor, and n runs from 0 to infinity. The function $f(E)$, with $W \ll \delta$, is sketched in the upper right corner of Fig. 6. Note that because the vibronic modes excited in C_{60} by a photoemission event are in fact more numerous[53] than the single mode contained in $f(E)$, this model function, while useful for extracting S_1 and T_1 amplitudes with a justifiable line shape, produces other parameters that are not intended for quantitative interpretation.

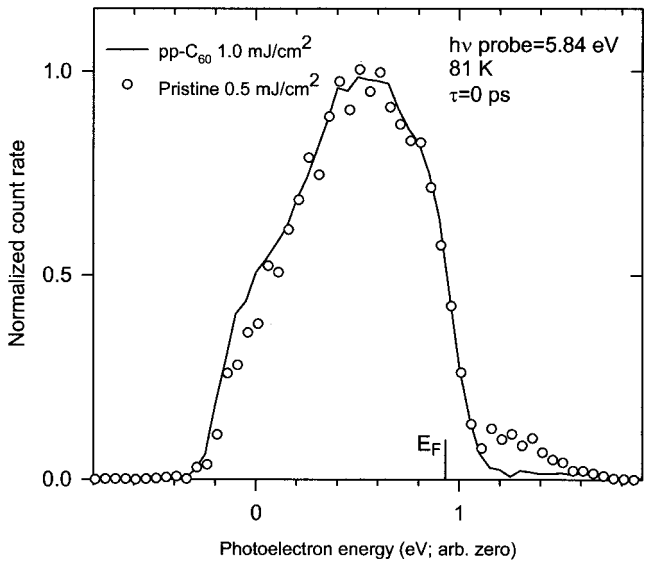

FIG. 8. Similarity of exciton spectra (background subtracted) for films of pristine (symbols) and photopolymerized (solid line) C_{60}. In both cases collision interactions have produced a significant T_1 contribution at zero probe delay τ. The Fermi level for both films occurred at E_F.

Secondary electrons were also approximately included in $f(E)$ by incorporating a "Shirley" background.[62] When fitting the full exciton band, the line shape parameters, including the relative strength of the background, were held fixed and only the amplitudes of the S_1 and T_1 components were varied, except that a small (~20% maximum) additional Gaussian broadening was allowed as fluence increased. The fitting could be improved by introducing an additional fluence-dependent emission at the lower energies, modeled here as a falling exponential and shown in the highest-fluence traces of Figs. 4 and 7. Time-resolved data taken with SR, where the entire HOMO was accessible, indicated this component could be ascribed to a fluence-dependent change in the shape of the upper limb of HOMO emission as discussed above. This change in shape is distinct from the small, rigid photovoltage. The association of this component with the tail of HOMO suggests it represents emission from ground-state molecules perturbed by proximal excited states.

Although low exciton concentrations in C_{60} have not been investigated because of small signals, the high-fluence spectrum for C_{60} is essentially identical to that of pp-C_{60}, as shown by Figs. 1 and 8. The pristine C_{60} spectrum in Fig. 8 can be satisfactorily fit with components shaped identically to those used in fitting pp-C_{60} in Figs. 3, 4, and 7. The time dependence of the C_{60} spectrum also shares general similarities with pp-C_{60}. As in pp-C_{60}, the higher energy component in C_{60} decays more rapidly, leaving a spectrum that behaves as T_1, as shown for LR in the inset to Fig. 1(b). Similarly, the shapes of the exciton emission measured with SR for C_{60} at 0.5 ns and 7.5 ns resembles those from pp-C_{60} at the same time delays (see Fig. 1; 7.5-ns pp-C_{60} spectrum is not shown). We conclude that the S_1 and T_1 components for C_{60} correspond closely to those for pp-C_{60}. This corre-

spondence is consistent with the resemblance of photoluminescence spectra, for which pp-C_{60} shows a very similar shape[50,51] and only a ~40 meV redshift (with comparable broadening)[51] compared to disordered pristine films. Evidently the states in pp-C_{60} responsible for broadening both the HOMO and LUMO to higher energy[27,34] perturb the exciton energies and splittings only slightly relative to our sensitivity.

Note, however, that details of the exciton dynamics differ in the two forms. In particular, at higher pump fluences the T_1 population in C_{60} decays significantly faster than in pp-C_{60}. Our analysis indicates this is a consequence of more effective interparticle annihilation collisions (see Sec. III C) among excited species in C_{60} at high concentrations, consistent with a higher mobility.[17] A higher mobility for excited states in C_{60} compared to pp-C_{60} may be attributable to greater disorder in pp-C_{60}, which exhibits varying intermolecular coordination and consequent bond disorder as noted above. Smaller exciton-exciton annihilation rates in pp-C_{60} due to reduced exciton mobility may also explain why we found excited-state signals to be larger in pp-C_{60} than in C_{60}.

B. Location of origin S_0

Our combined valence and exciton spectra provide an opportunity to determine the energy E_0 within the HOMO that serves as the origin of transitions: $E_0=\varepsilon_{00}-\Delta_{X0}$, where ε_{00} is the energy of the 0-0 photoemission line within the exciton spectrum, determined below, and Δ_{X0} is the 0-0 transition energy for creating an exciton, which is available from the literature. While the 0-0 photoemission line is spectrally unresolved, the vibrationally broadened line shapes of the exciton spectra indicate it should occur near the high-energy limb. Indeed, a detailed analysis[53] of photoemission from the HOMO of gas-phase C_{60} located the 0-0 line at the approximate midpoint of the upper limb, as marked in Fig. 5, and reasons were given for suspecting that the 0-0 line might actually be somewhat higher in energy. On the basis of the similarities in the shape and width of the exciton spectra compared to the HOMO spectrum from isolated C_{60}, Fig. 5, and the likelihood that excitons are localized primarily on one molecule, it is reasonable to expect the 0-0 line of an exciton to occur in the same relative position within its photoemission spectrum as does the 0-0 line for the gas-phase HOMO. We take this to be the case for both S_1 and T_1 in both pristine and polymerized samples. Hence the zero of energy employed in Figs. 1, 2, 4, and 7, which are referenced to ε_{00} of T_1, is taken at the midpoint of the upper limb of the T_1 spectrum.

The 0-0 transition energy Δ_{S0} for $S_0\rightarrow S_1$ is available from a number of measurements for pristine C_{60} as crystals and disordered films. One- and two-photon optical spectroscopies give $\Delta_{S0}=1.846$ eV for crystalline C_{60} at 10 K.[40] Second harmonic generation in evaporated films gives Δ_{S0} that varies from 1.81 eV at 295 K to 1.83 eV at 27 K.[63] Analyses of fluorescence from films and crystals have also yielded, respectively, 1.84 eV (temperature not reported)[37] and 1.871 eV (Ref. 47) at low temperatures. While specific measurements of Δ_{S0} appear not to have been reported for pp-C_{60}, a magnitude near that of C_{60} is probable since, as noted above, the fluorescence spectrum of pp-C_{60} is similar to that from disordered C_{60} films and is redshifted by only ~40 meV.[50,51]

There is greater uncertainty in the energy Δ_{T0} of the 0-0 transition for $S_0\rightarrow T_1$. (A number of distinct triplet states identified through magnetic resonance and phosphorescence have been reviewed[64] but are too closely spaced to be distinguished in the present experiments.) Phosphorescence from crystals at 1.2 K indicates triplet states at 1.44 and 1.50 eV.[65] A Δ_{T0} of 1.50 eV has also been reported for phosphorescence from films, presumably at room temperature.[37] $S_0\rightarrow T_1$ transitions have also been identified in EELS.[39,56,66–68] A Δ_{T0} of 1.55 eV was reported for films at room temperature.[39] A weak temperature dependence has been noted for the (111) surface of ordered films, with Δ_{T0} increasing from 1.53 eV at 300 K to 1.55 eV at 100 K.[56] Finally, for similar ordered films at 107 K, distinct energies have been proposed for surface and bulk T_1 states[67] (see below).

Given the range in reported values for Δ_{S0} and Δ_{T0}, it is reasonable for present purposes, though somewhat arbitrary, to infer from the above measurements values of $\Delta_{S0}=1.87$ eV and $\Delta_{T0}=1.54$ eV, with uncertainties ± 0.05 eV. These choices preserve our measured S_1-T_1 splitting of 0.33 eV. The resulting energy of the origin, i.e., $E_0=\varepsilon_{00}^{T}-\Delta_{T0}$, is labeled in Fig. 1 as S_0. It occurs at -1.54 eV since we reference our energies to ε_{00}^{T} located in the upper limb of the long-lived T_1 spectrum as discussed above. The origin falls on the high-energy side of the HOMO, which is emphasized when the HOMO photoemission obtained with higher energy resolution is considered [see dashed data in Fig. 1(b)]. (A shift in the apparent position of ε_{00}^{T}, if exciton data were taken with the same high energy resolution, is expected to be small since the 0-0 line is taken near the *midpoint* of the upper limb of the T_1 spectrum.) The location of S_0 is expected in the upper portion of the HOMO if significant vibrational broadening in the final state, comparable to that which broadens the exciton spectra, contributes to the HOMO photoemission.[53] Our location of S_0 is inconsistent with a recent interpretation of femtosecond ESPES data.[11] This interpretation, by assuming an origin at the *peak* of the HOMO, rather than in its *upper limb*, identified as S_1 what is actually the long-lived T_1 spectrum.

Because ESPES is both bulk and surface sensitive, as with any photoelectron spectroscopy, the question arises as to whether surface and bulk excitons can be distinguished. In van der Waals bonded materials, which generally lack strong one-electron surface states, several factors may still alter the surface exciton transition energy Δ_{srf} compared to that of the bulk, Δ_{blk}.[3] A tendency for Δ_{srf} to exceed Δ_{blk} should accompany the larger surface band gap that is expected when the decreased coordination at the surface narrows the HOMO and LUMO widths.[59,69] On the other hand, a *reduced* Δ_{srf} would accompany the increased exciton binding energy expected for less effective screening at the surface.[69,70] In van der Waals materials studied with optical methods, valence excitons have been reported with surface transition energies

$\sim$0.04 eV *greater* than the bulk (anthracene[71]) and $\sim$0.2 eV *less* than the bulk (rare gas solids[70,72]), as reviewed by Pope and Swenberg.[3] In the EELS experiment noted above,[67] a weak loss at 1.64 eV was attributed to a bulk T_1 state because, at low primary beam energy (1.9 eV) where electron penetration and escape depths increase, it exceeded in amplitude the 1.55-eV feature. However, such a large bulk energy appears to be inconsistent with $\Delta_{T0} \approx 1.50$ eV measured by phosphorescence, which is bulk sensitive.

In photoemission, another shift occurs inherently between surface and bulk features. The shift arises because the positively charged photohole induces different electronic polarization energies in the sample depending on the hole's location relative to the surface.[73,74] Because of this polarization difference, the electrostatic energy of any charged species *inside* a dielectric rises as the charge approaches the surface, much as the energy of a charge *outside* a dielectric (or metal) decreases as described approximately in terms of an image charge.[73,75] The surface polarization shift for C_{60} films has been treated experimentally and theoretically by Rotenberg *et al.*, who found that surface features shifted $\sim$0.1 eV toward smaller kinetic energy, as expected.[73] Note that ESPES of unbound electrons (i.e., molecular anions) is subject to an *opposite* shift between surface and bulk. In this case, the final state of the material is neutral but the negatively charged *initial* state possessed increased electrostatic energy at the surface. For surface sensitive ESPES, this energy increase for electrons near the surface would have to be considered when comparing the relative energies of exciton and electron spectra. Note that this polarization repulsion away from the surface for charged species inside a dielectric may decrease the sensitivity of ESPES to free electrons in molecular materials and semiconductors. The degree depends on temperature, photoelectron escape depth, material dielectric constant, and, in experiments that transiently pump the surface region, on dynamic parameters such as hopping times and mobility that control movement away from the surface. Hence two effects may reduce ESPES sensitivity to bulk free electrons: polarization repulsion from the surface, and a smaller cross section accompanying delocalization[46] as discussed above.

The present data were acquired with photoelectron escape depths that should emphasize bulk features over surface ones. The combined T_1 and S_1 exciton spectra acquired with LR were centered at a kinetic energy about 0.7 eV above the vacuum level, for which the photoelectron attenuation length exceeds 2 nm according to measurements of the attenuation of substrate core levels[76] and to measurements reported by Goldoni *et al.*[56] Using a lower limit of 2 nm for an electron attenuation length, and a 0.8-nm separation between (111) planes[77] as a gauge of the spacing between molecular layers parallel to the surface, we find that surface molecules would represent less than $\frac{1}{3}$ of our signal if all other factors were equal. However, we find no evidence of distinct surface and bulk exciton components although the existence of such components with small relative amplitudes or splittings cannot be ruled out.

C. Fluence and time dependence

In Figs. 3 and 4, the shapes of the exciton spectra for pp-C_{60} are shown evolving with increasing incident pump fluence as measured with LR at 0 time delay τ between pump and probe. Fluence-dependent data were routinely checked for irreversible laser-induced changes by periodically returning to low-fluence conditions. Occasionally, changes in amplitude up to $\sim$20% were observed over the course of several hours. Since these changes could be either positive or negative, experimental instabilities are a possibility. Systematic biases due to possible changes in sample condition were reduced by varying the pump fluence nonmonotonically in any given series of measurements.

The similarity of the fluence-dependent spectra recorded at 81 K and room temperature is evident by comparing Figs. 3 and 4. T_1 and S_1 components, obtained through line fitting as described above, are shown as dashed and solid lines, respectively. In Fig. 3, the intensities of these fitted S_1 and T_1 components are plotted in the inset as symbols. In both Figs. 3 and 4, the spectrum at lowest fluence is almost entirely S_1. The concentration, in the low-to-mid $10^{18}\,\mathrm{cm}^{-3}$ range, is too small for excited-state interactions to introduce significant nonlinearities. However, as the concentration of nonequilibrium species increases, it is evident that a preferential conversion of incident energy to the T_1 population occurs until, at the highest fluence, the S_1 population exhibits a saturating behavior while the T_1 population continues to grow.

In the inset to Fig. 3, the measured S_1 and T_1 fluence-dependent intensities (symbols) are reproduced, respectively, by solid and dashed curves. These curves give the fluence dependence as predicted by a model comprising three rate equations to account for interacting populations of S_1, T_1, and free carriers (F). The model, which has been discussed in a letter format,[17] will be elaborated elsewhere. In addition to reproducing the S_1 and T_1 fluence dependencies, the model also reproduces complex fluence-dependent transient decays of S_1 and T_1 that were recorded after the pump pulse. The ability of ESPES to spectrally separate the S_1 and T_1 *transient* behaviors is illustrated by the time-dependent series of spectra in Fig. 7, which was initiated by a relatively high incident fluence (1 $\mathrm{mJ/cm}^2$) that produced substantial triplet population even at zero delay.

The rate-equation model[17,78] is also able to reproduce the enhanced production of triplets observed at high fluence. Here we briefly note that this enhancement occurs through the spin-conserving manifolds of the interactions (i) $S+S \rightarrow T+T$ or (ii) $S+F \rightarrow T+F$. The former reaction (i) is analogous to well documented singlet fission in polyacenes, which differs in that one of the singlets is a ground state molecule.[3] An enhanced production of the T_1 population may still ensue if the two triplets formed in close proximity by interaction (i) subsequently annihilate through the channel $T+T \rightarrow T+S_0$.[2] Reaction (i) was previously suggested to operate in C_{60} to account for a transient absorption signal that decayed more rapidly as excitation fluence increased but that left a long-lived transient residue attributed to T_1 absorption.[19] Those experiments were carried out on films

exposed to air and were unable to separate overlapping S_1 and T_1 contributions, as our ESPES results do. Interaction (i) has also been invoked to explain increased T_1 production at high excitation densities observed by transient absorption in *para*-hexaphenyl films, in which separate absorptions from S_1, T_1, and polarons were followed.[2]

In reaction (ii), $S+F\rightarrow T+F$, a spin-$\frac{1}{2}$ mediated intersystem crossing[79] is induced by a free electron or hole. This interaction may be viewed as analogous to the (energetically disallowed) back reaction of the annihilation interaction[3] $T+F\rightarrow S_0+F$, which also results in an effective spin flip of the free carrier. The reaction $S+F\rightarrow T+F$ is energetically allowed, with energy conserved either by creation of vibrations or by the free-carrier taking up the $\sim$0.3 eV of S_1-T_1 splitting. The back-reaction rates of (i) and (ii), $S+S\leftarrow T+T$ and $S+F\leftarrow T+F$, require $\sim$0.6 and $\sim$0.3 eV, respectively, and are energetically unfavorable at our temperatures. The model finds that nongeminate recombination of electrons and holes, for which spin statistics favor triplet formation as $F+F\rightarrow 0.75T+0.25S$, contributes to T_1 production only slightly, in part because free carriers are formed inefficiently in C_{60}.[42,43] The slight contribution discounts the effect of any adjustment in the spin-statistical branching ratio that cross section effects may impart.[80]

Biparticle interactions also cause a rapid decay of S_1 at high concentrations. This is clearly evident in Fig. 7 for pp-C_{60} at 81 K pumped with 1 mJ/cm^2. Only 10% of the peak S_1 population remains after 200 ps, a time much less than the unimolecular decay time of $\sim$1.3 ns we measure at *low* fluence. Very similar behavior was measured for films at room temperature. Contributing to the rapid S_1 decay are the annihilation interactions $S+S\rightarrow S_0+S$ and $S+T\rightarrow S_0+T$, the latter of which drives the S_1 population to low values as the T_1 population is enhanced at high excitation density.

IV. SUMMARY

By employing excited-state photoelectron spectroscopy (ESPES), we have investigated laser-pumped exciton states in films of C_{60} and photopolymerized C_{60} (pp-C_{60}). Use of both synchrotron and laser probes permitted time scales to extend from 10's of picoseconds, much less than the unimolecular lifetime of the lowest lying singlet exciton (S_1), to more than 10 μs, when only triplet states (T_1) remain. Larger signals in pp-C_{60} enabled detailed studies, including the temporal isolation of each of the identically shaped T_1 and S_1 spectra and their identification that corrects a previous assignment.[11] Our assignments of T_1 and S_1 spectra is supported by (i) their widely disparate lifetimes being in accord with general expectations and the literature, (ii) a splitting in accord with the literature, (iii) identical line shapes, and (iv) location of both below the Fermi level.

The T_1 state was measured to lie 0.33 eV below S_1 in pp-C_{60} but the two spectra nevertheless overlap because of significant vibrational broadening in the photoemission final state. Vibrational broadening is verified by the close correspondence in shape and width between our exciton spectra and vibrationally broadened photoemission spectra from isolated C_{60} molecules.[53] The correspondence guided our placement of the 0-0 photoemission transition on the upper limbs of the exciton spectra.

For pump fluences that create exciton concentrations $\gtrsim 10^{19}$ cm^{-3}, we found the unexpected result that the T_1 population predominates over the S_1 population on a time scale faster than our 50-ps probe resolves. This time is much less than the $\sim$2.5-ns intersystem crossing time we measure at lower exciton concentrations. Similar behavior has been previously suggested[19] for incompletely characterized films of C_{60} and has also been discovered in model compounds of conjugated polymers.[2] Excess T_1 production at high concentrations may have ramifications for potential devices operating at high concentrations, such as polymeric lasers. When the separate dynamics of both S_1 and T_1 populations are followed over wide fluence and time regimes, we have found it necessary to adopt a more comprehensive rate-equation model than previously applied, one which incorporates interactions among all three primary excited species, namely, S_1 and T_1 excitons and charged carriers.

The weaker spectra from pristine C_{60} were examined at our higher incident pump fluences where, as in pp-C_{60}, excited-state interactions led to the unavoidable predominance of triplets. The resulting exciton spectrum from C_{60} was indistinguishable from pp-C_{60} within noise constraints. The two forms also exhibited similar transient behavior but with faster bimolecular decays in C_{60}, attributable to larger mobilities and correspondingly larger interaction rates. By employing the reported transition energies for creating S_1 and T_1 states in C_{60}, and noting the similar spectral characteristics of excitons in the two forms, we are able to locate the apparent origin of transitions in photoemission spectra of both C_{60} and pp-C_{60} to be within the upper limb of the HOMO, rather than its center. This result is consistent with vibrational broadening making a significant contribution to the width of the HOMO photoemission spectrum in addition to any dispersive broadening.

ACKNOWLEDGMENTS

We gratefully acknowledge important contributions to the synchrotron experiments from Bruce Itchkawitz, Thomas Schedel-Niedrig, Roger Klaffky, Bill Hunter, and Jack Rife. We are also indebted to Bill Hunter for thin-film optical calculations. This work was supported by the Naval Research Laboratory which is funded by the Office of Naval Research. The National Synchrotron Light Source at Brookhaven National Laboratory is supported by the U.S. Department of Energy.

*Present address: 18608 Beardslee Blvd., G202, Bothell, WA 98011.
[1] M. A. Baldo, D. F. O'Brien, M. E. Thompson, and S. R. Forrest, Phys. Rev. B **60**, 14 422 (1999).
[2] C. Zenz, G. Cerullo, G. Lanzani, W. Graupner, F. Meghdadi, G. Leising, and S. De Silvestri, Phys. Rev. B **59**, 14 336 (1999).
[3] M. Pope and C. E. Swenberg, *Electronic Processes in Organic Crystals and Polymers* (Oxford University Press, New York, 1999).
[4] S. L. Dexheimer, in *Optical and Electronic Properties of Fullerenes and Fullerene-Based Materials*, edited by J. Shinar, Z. V. Vardeny, and Z. H. Kafafi (Marcel Dekker, New York, 2000), p. 21.
[5] W. R. Salaneck, H. W. Gibson, E. W. Plummer, and B. H. Tonner, Phys. Rev. Lett. **49**, 801 (1982).
[6] E.-E. Koch, Phys. Scr. **T17**, 120 (1987).
[7] R. Haight, Surf. Sci. Rep. **21**, 275 (1995).
[8] H. Petek and S. Ogawa, Prog. Surf. Sci. **56**, 239 (1997).
[9] B. S. Itchkawitz, J. P. Long, T. Schedel-Neidrig, W. R. Hunter, R. Schoegl, A. M. Bradshaw, and M. N. Kabler, in *Proceedings of the 22nd International Conference on Physics of Semiconductors*, edited by D. J. Lockwood (World Scientific, Singapore, 1995).
[10] S. J. Chase, J. P. Long, B. S. Itchkawitz, and M. N. Kabler, Bull. Am. Phys. Soc. **41**, 131 (1996).
[11] R. Jacquemin, S. Kraus, and W. Eberhardt, Solid State Commun. **105**, 449 (1998).
[12] M. Probst and R. Haight, Appl. Phys. Lett. **71**, 202 (1997).
[13] G. D. Hale, S. J. Oldenburg, and N. J. Halas, Phys. Rev. B **55**, R16 069 (1997).
[14] T. Quast, R. Bellmann, B. Winter, J. Gatzke, and I. V. Hertel, J. Appl. Phys. **83**, 1642 (1998).
[15] A. J. Mäkinen, S. Xu, Z. Zhang, S. J. Diol, Y. Gao, M. G. Mason, A. A. Muenter, D. A. Mantell, and A. R. Melnyk, Appl. Phys. Lett. **74**, 1296 (1999).
[16] S. Link, A. Scholl, R. Jacquemin, and W. Eberhardt, Solid State Commun. **113**, 689 (2000).
[17] J. P. Long, S. J. Chase, and M. N. Kabler, Chem. Phys. Lett. **347**, 29 (2001).
[18] J. P. Long, Nucl. Instrum. Methods Phys. Res. A **266**, 673 (1988).
[19] T. N. Thomas, R. A. Taylor, J. F. Ryan, D. Mihailovic, and R. Zamboni, Europhys. Lett. **25**, 403 (1994).
[20] S. R. Flom, F. J. Bartoli, H. W. Sarkas, C. D. Merrit, and Z. H. Kafafi, Phys. Rev. B **51**, 11 376 (1995).
[21] J. P. Long, B. S. Itchkawitz, and M. N. Kabler, J. Opt. Soc. Am. B **13**, 201 (1996).
[22] P. J. Benning, D. M. Poirier, N. Troullier, J. L. Martins, and J. H. Weaver, Phys. Rev. B **44**, 1962 (1991).
[23] Y. B. Xu, M. Q. Tan, and U. Becker, Phys. Rev. Lett. **76**, 3538 (1996).
[24] W. R. Hunter and J. P. Long, Appl. Opt. **33**, 1264 (1994).
[25] D. Eimerl, L. Davis, S. Velsko, E. K. Graham, and A. Zalkin, J. Appl. Phys. **62**, 1968 (1987).
[26] SES Research Inc., 99.99% stated purity.
[27] B. S. Itchkawitz, J. P. Long, T. Schedel-Niedrig, M. N. Kabler, A. M. Bradshaw, R. Schloegl, and W. R. Hunter, Chem. Phys. Lett. **243**, 211 (1995).
[28] W. F. Krolikowski and W. E. Spicer, Phys. Rev. B **1**, 478 (1970).
[29] PDE Solutions, Inc.
[30] R. C. Yu, N. Tea, M. B. Salamon, D. Lorents, and R. Malhotra, Phys. Rev. Lett. **68**, 2050 (1992).
[31] V. D. Blank, S. G. Buga, N. R. Serebryanaya, G. A. Dubitsky, R. H. Bagramov, M. Y. Popov, V. M. Prokhorov, and S. A. Sulyanov, Appl. Phys. A: Mater. Sci. Process. **64**, 247 (1997).
[32] J. H. Apfel, Appl. Opt. **15**, 2339 (1976).
[33] J. P. Long, H. R. Sadeghi, J. C. Rife, and M. N. Kabler, Phys. Rev. Lett. **64**, 1158 (1990).
[34] M. R. Pederson and A. A. Quong, Phys. Rev. Lett. **74**, 2319 (1995).
[35] P. C. Ecklund, A. M. Rao, P. Zhou, Y. Wang, and J. M. Holden, Thin Solid Films **257**, 185 (1995).
[36] M. S. Dresselhaus and G. Dresselhaus, Annu. Rev. Mater. Sci. **25**, 487 (1995).
[37] S. Kazaoui, N. Minami, Y. Tanabe, H. J. Byrne, A. Eilmes, and P. Petelenz, Phys. Rev. B **58**, 7689 (1998).
[38] E. L. Shirley, L. X. Benedict, and S. G. Louie, Phys. Rev. B **54**, 10 970 (1996).
[39] G. Gensterblum, J. J. Pireaux, P. A. Thiry, R. Caudano, J. P. Vigneron, P. Lambin, A. A. Lucas, and W. Krätschmer, Phys. Rev. Lett. **67**, 2171 (1991).
[40] H. Schlaich, M. Muccini, J. Feldmann, H. Bassler, E. O. Göbel, R. Zamboni, C. Taliani, J. Erxmeyer, and A. Weidinger, Chem. Phys. Lett. **236**, 135 (1995).
[41] R. W. Lof, M. A. van Veenendaal, B. Koopmans, H. T. Jonkman, and G. A. Sawatzky, Phys. Rev. Lett. **68**, 3924 (1992).
[42] J. Mort, M. Machonkin, I. Chen, and R. Ziolo, Philos. Mag. Lett. **67**, 77 (1993).
[43] R. Konenkamp, R. Engelhardt, and R. Henninger, Solid State Commun. **97**, 285 (1996).
[44] L. Onsager, Phys. Rev. **54**, 554 (1938).
[45] D. M. Pai and R. C. Enck, Phys. Rev. B **11**, 5163 (1975).
[46] D. Emin, Phys. Rev. B **48**, 13 691 (1993).
[47] W. Guss, J. Feldmann, E. O. Göbel, C. Taliani, H. Mohn, W. Müller, P. Häussler, and H.-U. ter Meer, Phys. Rev. Lett. **72**, 2644 (1994).
[48] V. Capozzi, M. Santoro, G. Celentano, H. Berger, and G. F. Lorusso, J. Lumin. **76–77**, 395 (1998).
[49] I. O. Bashkin, A. N. Izotov, A. P. Moravsky, V. D. Negrii, R. K. Nikolaev, Y. A. Ossipyan, E. G. Ponyatovsky, and E. A. Steinman, Chem. Phys. Lett. **272**, 32 (1997).
[50] U. D. Venkateswaran, D. Sanzi, A. M. Rao, P. C. Eklund, L. Marques, J.-L. Hodeau, and M. Nunex-Regueiro, Phys. Rev. B **57**, R3193 (1998).
[51] M. S. Dresselhaus, G. Dresselhaus, A. M. Rao, and P. C. Eklund, Synth. Met. **78**, 313 (1996).
[52] P. M. Pippenger, R. D. Averitt, V. O. Papanyan, P. Nordlander, and N. J. Halas, J. Phys. Chem. **100**, 2854 (1996).
[53] P. A. Brühwiler, A. J. Maxwell, P. Baltzer, S. Andersson, D. Arvanitis, L. Karlsson, and N. Mårtensson, Chem. Phys. Lett. **279**, 85 (1997).
[54] W. Hayes and A. M. Stoneham, *Defects and Defect Processes in Nonmetallic Solids* (Wiley, New York, 1985).
[55] M. Ueta, H. Kanzaki, K. Kobayashi, Y. Toyozawa, and E. Hanamura, *Excitonic Processes in Solids* (Springer-Verlag, Berlin, 1986).
[56] A. Goldoni, C. Cepek, and S. Modesti, Phys. Rev. B **54**, 2890 (1996).
[57] P. Rudolf, M. S. Golden, and P. A. Brühwiler, J. Electron. Spec-

trosc. Relat. Phenom. **100**, 409 (1999).
[58] G. Gensterblum, J. Electron. Spectrosc. Relat. Phenom. **81**, 89 (1996).
[59] G. K. Wertheim, Phys. Rev. B **51**, 10 248 (1995).
[60] P. J. Benning, C. G. Olson, D. W. Lynch, and J. H. Weaver, Phys. Rev. B **50**, 11 239 (1994).
[61] G. Gensterblum, J.-J. Pireaux, P. A. Thiry, R. Caudano, T. Buslaps, R. L. Johnson, G. Le Lay, V. Aristov, R. Günther, A. Taleb-Ibrahimi, G. Indlekofer, and Y. Petroff, Phys. Rev. B **48**, 14 756 (1993).
[62] D. A. Shirley, Phys. Rev. B **5**, 4709 (1972).
[63] A.-M. Janner, R. Eder, B. Koopmans, H. T. Jonkman, and G. A. Sawatzky, Phys. Rev. B **52**, 17 158 (1995).
[64] P. A. Lane, Z. V. Vardeny, and J. Shinar, in *Optical and Electronic Properties of Fullerenes and Fullerene-Based Materials*, edited by J. Shinar, Z. V. Vardeny, and Z. H. Kafafi (Dekker, New York, 2000).
[65] D. J. van den Heuvel, I. Y. Chan, E. J. J. Groenen, J. Schmidt, and G. Meijer, Chem. Phys. Lett. **231**, 111 (1994).
[66] C. Cepek, A. Goldoni, S. Modesti, F. Negri, G. Orlandi, and F. Zerbetto, Chem. Phys. Lett. **250**, 537 (1996).
[67] A. Goldoni, C. Cepek, and S. Modesti, Synth. Met. **77**, 189 (1996).
[68] A. Lucas, G. Gensterblum, J. J. Pireaux, P. A. Thiry, R. Caudano, J. P. Vigneron, P. Lambin, and W. Krätschmer, Phys. Rev. B **45**, 13 694 (1992).
[69] W. E. Pickett, in *Solid State Physics*, edited by H. Ehrenreich and F. Spaepen (Academic, Boston, 1993), Vol. 48, p. 226.
[70] G. Zimmerer, in *Excited-State Spectroscopy in Solids*, edited by U. M. Grassano and N. Terzi (North-Holland, Amsterdam, 1987), p. 37.
[71] M. R. Philpott and J.-M. Turlet, J. Chem. Phys. **64**, 3852 (1976).
[72] V. Saile and E. E. Koch, Phys. Rev. B **20**, 784 (1979).
[73] E. Rotenberg, C. Enkvist, P. A. Brühwiler, A. J. Maxwell, and N. Mårtensson, Phys. Rev. B **54**, R5279 (1996).
[74] W. R. Salaneck, in *Photon, Electron, and Ion Probes of Polymer Structure and Properties*, edited by D. W. Dwight, T. J. Fabish, and H. R. Thomas (American Chemical Society, Washington, D.C., 1981), Vol. 162, p. 121.
[75] J. D. Jackson, *Classical Electrodynamics* (Wiley, New York, 1962).
[76] J. E. Rowe (private communication).
[77] P. A. Heiney, J. E. Fischer, A. R. McGhie, W. J. Romanow, A. M. Denenstein, J. P. McCauley, A. B. Smith, and D. E. Cox, Phys. Rev. Lett. **66**, 2911 (1991).
[78] J. P. Long, S. J. Chase, and M. N. Kabler, Bull. Am. Phys. Soc. **46**, 1156 (2001).
[79] N. Toyama, M. Asano-Someda, T. Ichino, and Y. Kaizu, J. Phys. Chem. A **104**, 4857 (2000).
[80] M. Wohlgenannt, K. Tandon, S. Mazumdar, S. Ramesesha, and Z. V. Vardeny, Nature (London) **409**, 494 (2001).